

# Small calcification depiction in ultrasound B-mode images using decorrelation of echoes caused by forward scattered waves

Hirofumi Taki · Takuya Sakamoto ·  
Makoto Yamakawa · Tsuyoshi Shiina ·  
Kenichi Nagae · Toru Sato

Received: 17 September 2010/Accepted: 14 December 2010/Published online: 25 February 2011  
© The Japan Society of Ultrasonics in Medicine 2011

## Abstract

**Purpose** The purpose of this study is to propose a novel method to depict small calcifications in ultrasound B-mode images using decorrelation of forward scattered waves with no decrease in the frame rate.

**Methods** Since the waveform of an ultrasound pulse changes when it passes through a calcification location, the echo waveform from regions behind the calcification is quite different from that without a calcification. This indicates that the existence of a calcification is predictable based upon the waveform difference between adjacent scan lines by calculating cross-correlation coefficients. In addition, a high-intensity echo should return from the calcification itself. Therefore, the proposed method depicts the high-intensity echo positions with posterior low correlation coefficient regions.

**Results** Eleven of 15 wires 0.2–0.4 mm in diameter were depicted using this method, yielding a sensitivity of 73.3% and a specificity of 100%, even though they might go

undetected under clinical inspection of ultrasound B-mode images.

**Conclusion** This study suggests that an US device could perform well in terms of calcification detection.

**Keywords** Ultrasonography · Calcification · Decorrelation · Forward scattered wave · Calcification detection

## Introduction

Ultrasonography (US) has an excellent ability to depict soft tissues without ionizing radiation; however, the calcification detectability of US is insufficient compared with X-ray computed tomography (CT) and other X-ray imaging techniques [1–4]. The detection of calcification is an important factor when diagnosing the malignancy of masses. As such, improvement of the calcification detectability of US is strongly desired.

Since the echo from a calcification is supposed to be of high intensity, several calcification detection methods that use extraction of high-echo-intensity regions have been reported. For extraction of high-echo-intensity regions, many researchers have employed a constant false alarm rate (CFAR) technique [5, 6]. A CFAR detector extracts targets in nonstationary noise and clutter while maintaining a constant probability of a false alarm [7, 8]. Therefore, a small calcification with low echo intensity is almost never detected using CFAR detectors. In addition, when a layered structure exists close to a calcification, the specular echo from the layered structure severely interferes with detection of the calcification.

Other strategies to detect small calcifications employ techniques to suppress speckle artifacts. Tissue harmonic

H. Taki (✉) · T. Sakamoto · T. Sato  
Graduate School of Informatics, Kyoto University,  
Yoshida-honmachi, Sakyo-ku, Kyoto 606-8501, Japan  
e-mail: hirofumi.taki@mb6.seikyou.ne.jp

M. Yamakawa  
Advanced Biomedical Engineering Research Unit,  
Kyoto University, Yoshida-honmachi, Sakyo-ku,  
Kyoto 606-8501, Japan

T. Shiina  
Graduate School of Medicine, Kyoto University,  
Yoshida-honmachi, Sakyo-ku, Kyoto 606-8501, Japan

K. Nagae  
Corporate R&D HQ, Canon Inc, 30-2, Shimomaruko 3-chome,  
Ohta-ku, Tokyo 146-8501, Japan

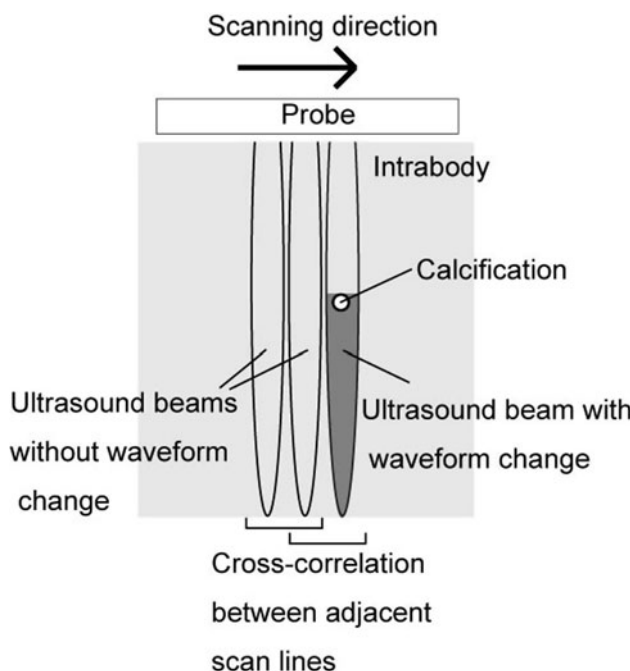


**Fig. 1** Schema of the proposed calcification depiction method using correlation coefficients between adjacent scan lines

imaging (THI) utilizes harmonics to suppress speckle artifacts [9–12]. However, THI exhibits considerably lower performance than CT in terms of calcification detection [1]. In contrast, spatial compound imaging generates a single B-mode image from multiple sweeps [13–16]. This causes the suppression of acoustic shadowing, resulting in the low performance of spatial compound imaging for calcification detection [17].

We have proposed a calcification detection strategy using cross-correlation between adjacent scan lines for detection of a small calcification with low echo intensity [18, 19]. Since the acoustic impedance of a calcification is much larger than that of other tissues, the waveform of an ultrasound wave changes significantly when it passes through the calcification location. This causes decorrelation between adjacent scan lines behind the calcification location, as shown in Fig. 1. Therefore, the existence of a calcification is predictable using the region with decorrelation that continues along the range direction, similar to calcification detection using acoustic shadowing. In addition, a relatively high intensity echo returns from a calcification because of its large acoustic impedance mismatch to soft tissue. In this study, we thus propose a method to presume the existence of calcifications by selecting high-echo-intensity positions with posterior low correlation regions. A layered structure behind a calcification improves the performance of the calcification depiction method [18]. Therefore, we investigate the performance of the proposed method experimentally under the condition that a layered structure exists just

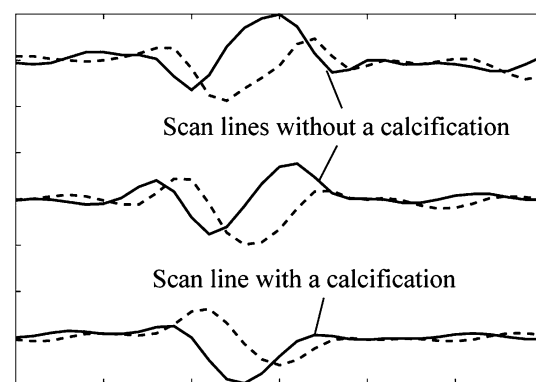


**Fig. 2** Waveforms of two scan lines of in-phase and quadrature data without a calcification and one scan line with a calcification. Solid and broken lines denote the waveforms of in-phase and quadrature data, respectively

behind a calcification, which is one of the most difficult cases in which to detect calcifications with US and suitable for the proposed calcification depiction method.

## Materials and methods

### Extraction of high-echo-intensity regions

An echo from a calcification should have a relatively high intensity because of its large acoustic impedance mismatch to soft tissue. For the selection of candidates for calcifications, the proposed method picks up positions where echo intensities exceed an intensity threshold,  $I_t$ . The condition of the cutaneous tissue layer influences the echo intensity in a region of interest behind the cutaneous layer. In contrast, two measurement regions of the same tissue have similar distribution shapes in terms of echo intensity. Therefore, the selection of candidates for calcifications should employ a rank filter, not a fixed echo intensity. We thus chose  $I_t$  as the intensity of a pixel that is a certain fraction of the maximum intensity value of the pixels in the image. The value of  $I_t$  depends on the echo intensity distribution of the measurement tissue, and the user should employ a value of  $I_t$  that is adequate to pick up all the pixels with sufficient intensities. In this study, we set  $I_t$  as 1% of the maximum intensity value of a pixel in a B-mode image.

### Correlation between adjacent scan lines

The proposed method utilizes correlation between adjacent scan lines for the depiction of calcifications. When a calcification exists in a scan line, creeping waves around the calcification surface, diffraction waves, and multiple reflection waves in the calcification occur in both the transmit and receive events. These forward scattered waves change the waveform considerably, as shown in Fig. 2. The

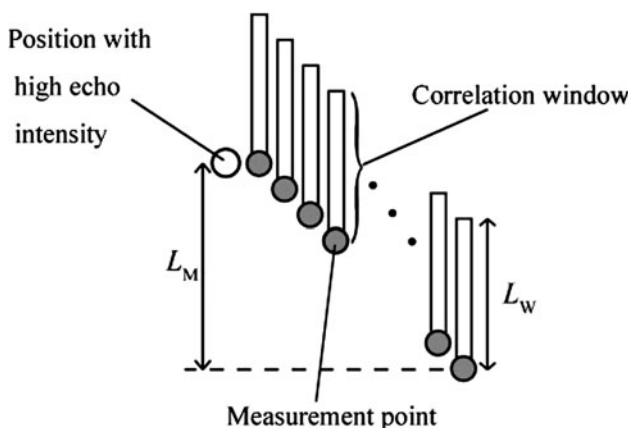


**Fig. 3** Measurement points behind a high-echo-intensity position investigated using the proposed method.  $L_w$  and  $L_M$  denote the correlation window width and the width of the measurement region behind the high-echo-intensity position, respectively

correlation of the echoes behind a calcification is thus suppressed severely. Since a calcification suppresses correlation of the region behind the calcification, the proposed method utilizes the measurement points behind a high-echo-intensity position where the correlation windows of the measurement points include the region behind the high-echo-intensity position, as shown in Fig. 3.

US devices acquire in-phase and quadrature (IQ) data for detection of the Doppler signal, and most devices utilize quadrature detectors for acquisition of IQ data. Detection is accomplished by mixing the received signal with two sinusoidal waves, where the phase difference of the two sinusoidal waves is  $90^\circ$  and their center frequency is equal to the transmit center frequency. A cross-correlation coefficient between adjacent scan lines of IQ data is suppressed not only by the existence of a calcification but also by the noise intensities of the scan lines. We thus employed an echo intensity constraint to suppress the influence of noise. The cross-correlation coefficient with a constraint is given by

$$r\left(x + \frac{\Delta X}{2}, z\right) = \max_L \frac{\left| \sum_{z'=z-L_w}^z g(x, z')g(x + \Delta X, z' + L\Delta Z)^*\right|}{\sqrt{\sum_{z'=z-L_w}^z |g(x, z')|^2 \sum_{z'=z-L_w}^z |g(x + \Delta X, z' + L\Delta Z)|^2}}, \quad (1)$$

subject to

$$\sqrt{\sum_{z'=z-L_w}^z |g(x, z')|^2} \sum_{z'=z-L_w}^z |g(x + \Delta X, z' + L\Delta Z)|^2 \geq \alpha m I_t, \quad (2)$$

where  $x$  and  $z$  are respectively the lateral and vertical components of a measurement point in a B-mode image,  $g(x, z)$  is

the IQ datum at a pixel in a B-mode image,  $g(x, z)^*$  is the complex conjugate of  $g(x, z)$ ,  $\Delta X$  is the scan line interval,  $\Delta Z$  is the range interval,  $\alpha$  is a positive number employed for the echo intensity threshold, and  $L_w$  and  $m$  are the width and number of pixels of the correlation window, respectively. The variable  $L$  is employed to acquire the maximum of the correlation coefficients. The correlation coefficient is normalized by the average echo intensity, and thus it relates to the waveform change itself. In this study, we examined cases of  $\alpha = 0.05, 0.1$ , and  $0.2$ . We set the correlation window width,  $L_w$ , and the width of the measurement region behind a high-echo-intensity position,  $L_M$ , to 5 and 6 mm, respectively. Since the range interval is 0.05 mm, the number of pixels of the correlation window is 100. In the cases of  $\alpha = 0.05, 0.1$ , and  $0.2$ , the method eliminates the cross-correlation coefficients with the echo intensity under 5, 10, and 20 times the echo intensity threshold,  $I_t$ , respectively. Since  $I_t$  is the echo intensity of a single pixel with a sufficient intensity, the echo cut out by the correlation window seldom has an echo intensity over 40 times  $I_t$ . In contrast, the echo intensity under twice  $I_t$  indicates an insufficient signal-to-noise ratio of the echo, and the echo should be eliminated. Therefore, the values of  $\alpha$  are adequate, and optimization of the values of  $\alpha$  is not necessary.

#### Depiction of high-echo-intensity positions with posterior low correlation regions

A calcification originates a high-echo-intensity position accompanied by a low correlation region behind the position. Therefore, the present method presumes the calcification positions by selecting the high-echo-intensity positions with posterior low correlation regions. First, the method calculates the ratio of correlation coefficients lower than the value of a correlation threshold among the measurement region behind each high-echo-intensity position. The correlation threshold of  $\mu - \beta\sigma$  is determined using the average,  $\mu$ , and the standard deviation,  $\sigma$ , of the correlation coefficients of all the measurement regions behind all the high-echo-intensity positions, where  $\beta$  is a positive number. Then, the method depicts the high-echo-intensity position with a posterior low correlation region, where the region accounts for half the measurement region behind the high-echo-intensity position. In this study, we examined two cases, i.e.,  $\beta = 2$  and 3, because they are adequate statistically.

#### Experimental setup

Experiments were conducted with a Hitachi EUB-8500 (Hitachi, Tokyo, Japan) US device, which has a function to export raw IQ data. A 7.5-MHz linear array probe was used, where the scan line interval,  $\Delta X$ , and range interval,  $\Delta Z$ , of the device were 0.13 and 0.05 mm, respectively. We



**Fig. 4** Calcification phantom prepared in this study

prepared a calcification phantom with three different copper wires (0.2, 0.29, and 0.4 mm in diameter from left to right) embedded into a 4% agar gel block at 2 cm depth and 1 cm intervals, as shown in Fig. 4. A polyethylene sheet 0.1 mm thick was placed just behind the wires. The agar gel contained 0.5% Tech Polymer particles, spherical polymer particles 7  $\mu\text{m}$  in diameter (Sekisui Plastics). Aberrations originating at a cutaneous tissue layer deteriorate the image quality of B-mode images, causing interference of calcification detection. To evaluate the influence of a cutaneous tissue layer, we placed a swine cutaneous tissue layer 1 cm thick onto the gel block. To avoid multiple reflections in the wires, the image plane was set at 85° to the wires. Figure 5 shows a B-mode image of the calcification phantom. In this set up, the specular echo from a polyethylene sheet had a higher intensity than that from wires, indicating that the strategy of selecting high-echo-intensity masses, such as CA CFAR detectors, was unsuitable for small calcification detection. Kamiyama et al. [6] focused on the tissue structure in a B-mode image having continuity in the lateral direction, and they proposed a calcification detection method using CA CFAR with a kernel that emphasizes the lateral direction. The cell averaging process employed by the method calculates the indicator of calcification:

$$P_{\text{CA}}(x, y) = P_L(x, y) - P_K(x, y), \quad (3)$$

where  $P_L(x, y)$  is the logarithmic intensity of a measurement pixel, and  $P_K(x, y)$  is the average of the logarithmic intensity of the kernel pixels surrounding the measurement pixel. However, the calcification detection ability of the method deteriorates when a layered structure is not parallel to the lateral direction and the echo intensity of the layered structure varies, as shown in Fig. 6.

In the present study, five B-mode images of different sections were obtained. Each B-mode image contained

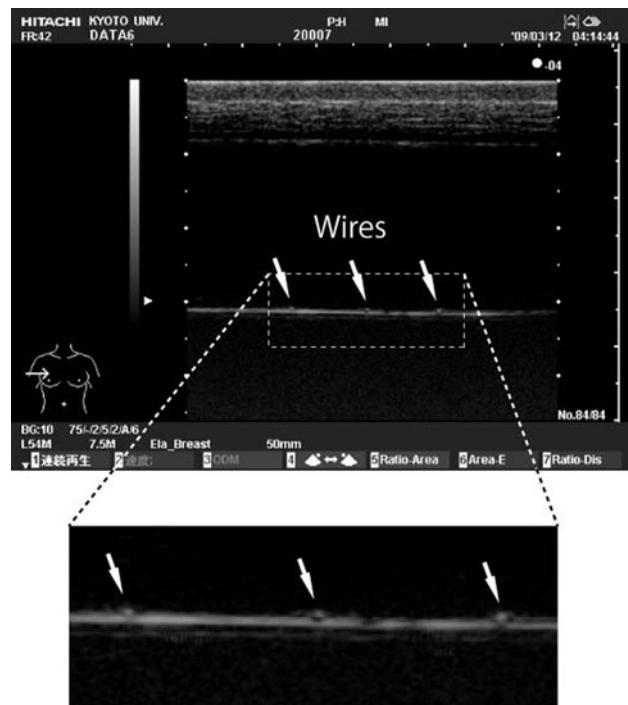


**Fig. 5** B-mode image of the calcification phantom with a swine cutaneous tissue layer. *White arrows* point to wires simulating calcifications

three wires, and thus the sum of the embedded wires was 15. To investigate the robustness of the proposed method, we also prepared a calcification phantom without a swine cutaneous tissue layer. As shown in Fig. 7, absence of a swine tissue layer was far from in vivo conditions, and the wires were easily detected upon US inspection.

## Results and discussion

### Calcification depiction using low correlation of adjacent scan lines

First, the proposed method selects high-echo-intensity positions in a B-mode image of a calcification phantom. As shown in Fig. 8, almost all specular echoes and echoes from wires were picked up by using the 1% intensity threshold. This indicates the validity of the echo intensity threshold for the calcification phantom. Then, the method calculates correlation coefficients in the measurement region behind the high-echo-intensity positions. Figure 9 shows correlation coefficients between adjacent scan lines, where three values of the intensity threshold,  $\alpha$ , were examined. The employment of a low value for  $\alpha$  means that the method counts scan lines with low SNR among the region for the calculation of correlation coefficients, causing enhancement of the influence of noise on the

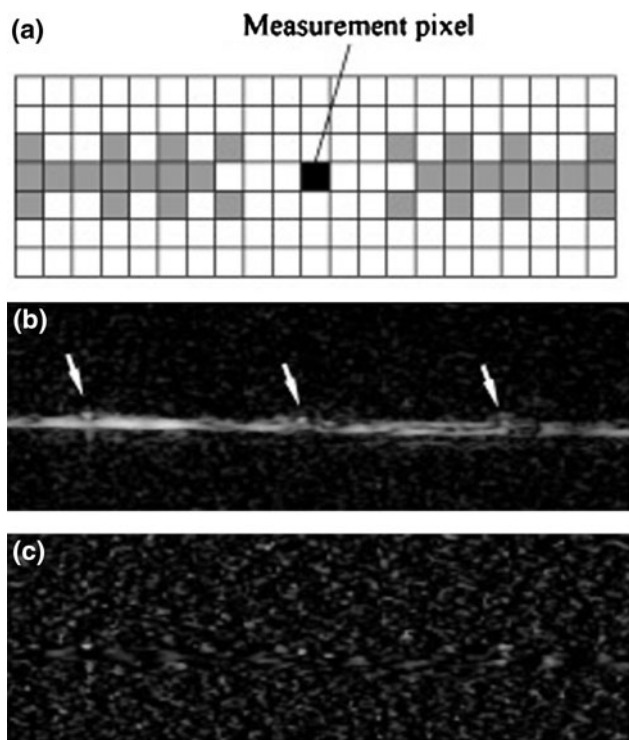


**Fig. 6** **a** Kernel pattern that emphasizes the lateral direction [6]. **b** B-mode image of the calcification phantom, and **c** that with the cell averaging process using the kernel. Gray pixels denote the kernel pixels, and the white arrows point at wires

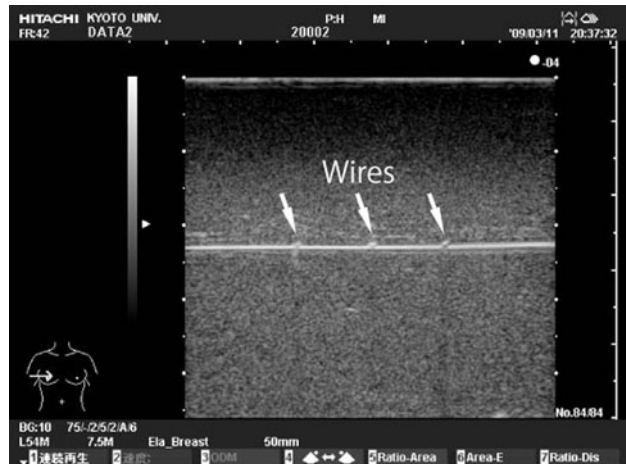


**Fig. 7** B-mode image of the calcification phantom without a swine cutaneous tissue layer

correlation profile. When  $\alpha$  of 0.05 was employed, correlation coefficients were suppressed continuously along the range direction behind the middle and right wires. When  $\alpha = 0.2$  was employed, false images were eliminated and the suppression of correlation coefficients caused by the left wire became conspicuous at a cost of the loss of the low correlation region caused by the right wire. In addition,

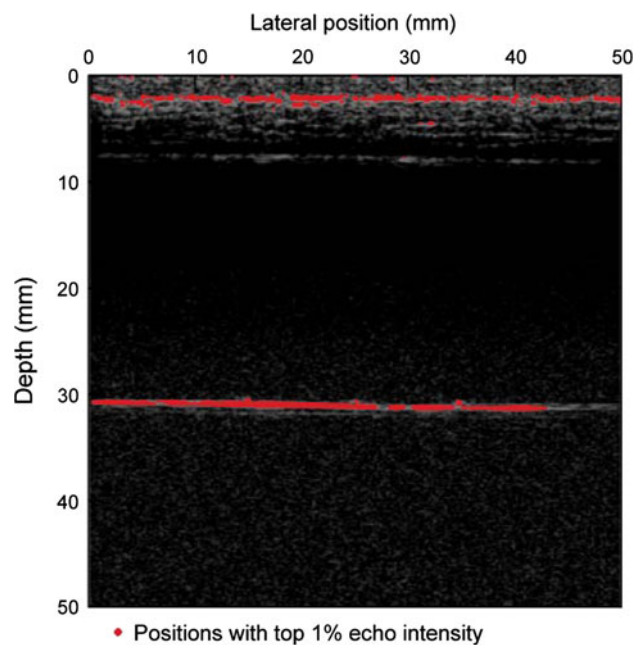


**Fig. 8** Candidates for wire positions with high echo intensities. The intensity threshold was set to the top 1% intensity threshold

the strong suppression of the correlation coefficients appeared only behind the wire positions, indicating that the employment of a high correlation threshold can eliminate false images at the cost of the sensitivity of the method. When a correlation threshold parameter  $\beta$  of 3 was employed, i.e., the correlation threshold of  $\mu - 3\sigma$  was employed, no false image appeared in this study. Therefore, a correlation threshold parameter  $\beta$  over 3 is useless under the conditions of this study.

#### Calcification depiction with a totalizing process

The degree of suppression in a correlation profile caused by a wire depends on the intensity threshold parameter  $\alpha$ , as shown in Fig. 9. Therefore, we propose a calcification depiction method with a totalizing process. First, the method calculates three correlation profiles using three values for  $\alpha = 0.05, 0.1$ , and  $0.2$ , where each profile uses a certain value for  $\beta$ . After the selection of calcification positions in the three correlation profiles, the method totals up all the selected positions and depicts them on the B-mode image.

When the method employs a small value for  $\beta$ , i.e., when a mild correlation threshold is employed, the sensitivity of the method improves at the cost of the appearance of false images. Since a correlation profile using a large value for  $\alpha$  is less influenced by noise, a false image rarely appears in the profile. To improve the performance of the method, we employed a smaller value for  $\beta$  for the

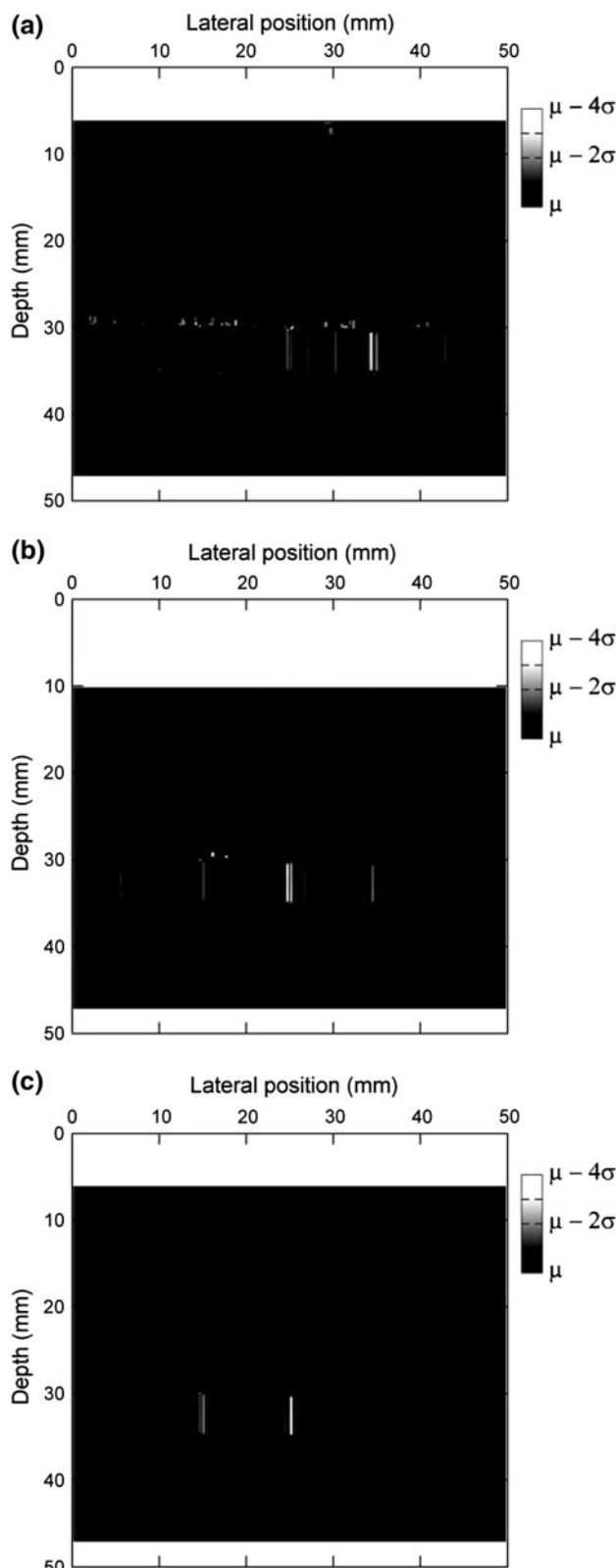


**Fig. 9** Correlation profiles between adjacent scan lines employing three values of the intensity threshold parameter  $\alpha$  = **a** 0.05, **b** 0.1, and **c** 0.2

**Table 1** Threshold sets of three combinations of parameters  $\alpha$  and  $\beta$  employed by the proposed calcification depiction method with a totalizing process

Threshold number	Combinations of parameters $\alpha$ and $\beta$
1	$(\alpha, \beta) = (0.05, 3), (0.1, 3), (0.2, 3)$
2	$(\alpha, \beta) = (0.05, 3), (0.1, 3), (0.2, 2)$
3	$(\alpha, \beta) = (0.05, 3), (0.1, 2), (0.2, 2)$
4	$(\alpha, \beta) = (0.05, 2), (0.1, 2), (0.2, 2)$

selection of calcification positions in a correlation profile with a larger value of  $\alpha$ . As the employment of  $\beta$  over 3 is useless under the conditions of this study, we examined two cases, i.e.,  $\beta = 2$  and 3. Table 1 shows the four threshold sets utilized by the proposed calcification depiction method with a totalizing process, where a prior threshold number denotes a more severe threshold. As expected, employing a milder threshold yielded a higher sensitivity at the cost of the positive predictive value, as shown in Fig. 10. We calculated the sensitivity and the positive predictive value (PPV) of the method as  $N_D/N_T$  and  $N_D/(N_D + N_{FP})$ , respectively, where  $N_D$ ,  $N_T$ , and  $N_{FP}$  are the number of detected wires, embedded wires, and false-positive wires, respectively. In this study, three wires were embedded in a phantom, i.e.,  $N_T = 3$ . The sensitivity and PPV are presented as the mean  $\pm$  standard deviation, where the number of samples is 5. The proposed calcification depiction method with the second threshold set depicted 11 of 15 wires embedded in five B-mode images of a phantom with a swine tissue layer, and all positions selected by the proposed method were located close to wires, as shown in Fig. 11, corresponding to a sensitivity of  $73.3 \pm 27.9\% (n=5)$  and a PPV of  $100 \pm 0\% (n=5)$ . When PPV = 100%, the number of false-positive wires is 0; and thus the specificity also becomes 100%. This result suggests that the proposed calcification depiction has the potential to depict thin wires about 0.3 mm in diameter with both high sensitivity and good specificity.

Applied to a phantom without a swine tissue layer, the proposed methods with a totalizing process had high sensitivities with sufficient PPV. These results show that the proposed method has a high sensitivity and a good PPV for small calcification detection with sufficient robustness.

## Conclusion

We propose a novel calcification depiction method that utilizes the decorrelation of forward scattered waves caused by the waveform change originating at a calcification

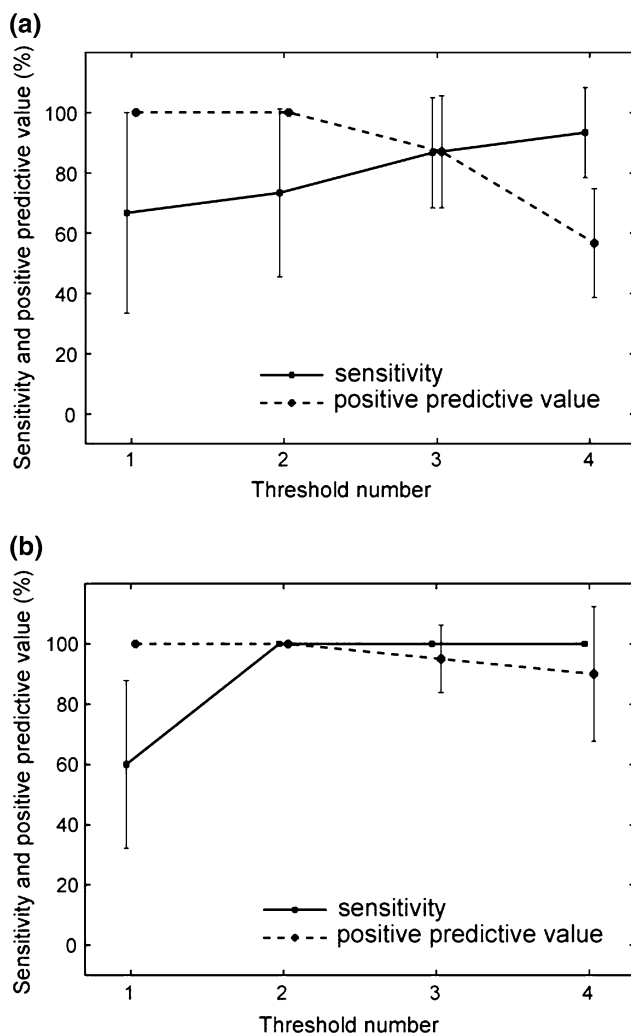


**Fig. 10** Sensitivity and positive predictive value of the proposed calcification depiction method with a totalizing process for a calcification phantom **a** with and **b** without a swine cutaneous tissue layer

location. A small calcification slightly changes the intensity of an ultrasound pulse causing no associated acoustic shadowing. However, it should change the waveform of the ultrasound pulse significantly. The proposed calcification depiction method depicted wires about 0.3 mm in diameter with a sensitivity of 73.3% and a specificity of 100%, where the wires might have gone undetected under clinical inspection of ultrasound B-mode images. This study suggests the probability that an US device will be able to perform calcification detection well. We investigated a situation where a single layered structure with calcifications exists in a homogeneous medium, simulating the calcifications in a gallbladder wall. Future work will examine a situation where calcifications and several layered structures exist in an inhomogeneous medium to investigate the

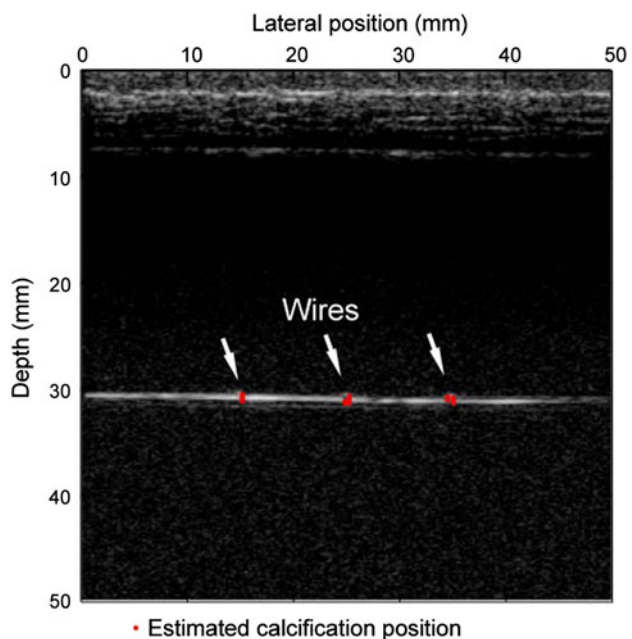


**Fig. 11** Estimated wire positions in a calcification phantom with a swine tissue layer, where the proposed method with a totalizing process employed the second threshold set

potential for application of the proposed method to breast cancer screening.

**Acknowledgments** This work is partly supported by the Research and Development Committee Program of the Japan Society of Ultrasonics in Medicine and the Innovative Techno-Hub for Integrated Medical Bio-imaging Project of the Special Coordination Funds for Promoting Science and Technology from the Ministry of Education, Culture, Sports, Science and Technology (MEXT), Japan.

## References

- Özdemir H, Demir MK, Temizöz O, et al. Phase inversion harmonic imaging improves assessment of renal calculi: a comparison with fundamental gray-scale sonography. *J Clin Ultrasound*. 2008;36:16–9.
- Fowler KAB, Locken JA, Duchesne JH, et al. US for detecting renal calculi with nonenhanced CT as a reference standard. *Radiology*. 2002;222:109–13.
- Lamb PM, Perry NM, Vinnicombe SJ, et al. Correlation between ultrasound characteristics, mammographic findings and histological grade in patients with invasive ductal carcinoma of the breast. *Clin Radiol*. 2000;55:40–4.
- Jacob D, Brombart JC, Muller C, et al. Analysis of the results of 137 subclinical breast lesions excisions. Value of ultrasonography in the early diagnosis of breast cancer. *J Gynecol Obstet Biol Reprod (Paris)*. 1997;26:27–31.
- Zhu Y, Weight JP. Ultrasonic nondestructive evaluation of highly scattering materials using adaptive filtering and detection. *IEEE Trans Ultrason Ferroelect Freq Contr*. 1994;41:26–33.
- Kamiyama N, Okamura Y, Kakee A, et al. Investigation of ultrasound image processing to improve perceptibility of microcalcifications. *J Med Ultrasonics*. 2008;35:97–105.

7. Finn HM, Johnson RS. Adaptive detection mode with threshold control as a function of spatially sampled clutter-level estimates. *RCA Rev.* 1968;29:414–65.
8. Hansen VG, Ward HR. Detection performance of the cell averaging LOG/CFAR receiver. *IEEE Trans Aerosp Electron Syst.* 1972;5:648–52.
9. Schmidt T, Hohl C, Haage P, et al. Diagnostic accuracy of phase-inversion tissue harmonic imaging versus fundamental B-mode sonography in the evaluation of focal lesions of the kidney. *AJR Am J Roentgenol.* 2003;180:1639–47.
10. Rosenthal SJ, Jones PH, Wetzel LH. Phase inversion tissue harmonic sonographic imaging: a clinical utility study. *AJR Am J Roentgenol.* 2001;176:1393–8.
11. Szopinski KT, Pajk AM, Wysocki M, et al. Tissue harmonic imaging: utility in breast sonography. *J Ultrasound Med.* 2003;22:479–87.
12. Rosen EL, Soo MS. Tissue harmonic imaging sonography of breast lesions improved margin analysis, conspicuity, and image quality compared to conventional ultrasound. *Clin Imaging.* 2001;25:379–84.
13. Krücker JF, Meyer CR, LeCarpentier GL, et al. 3D spatial compounding of ultrasound imaging using image-based nonrigid registration. *Ultrasound Med Biol.* 2000;26:1475–88.
14. Moskalik A, Carson PL, Meyer CR, et al. Registration of 3-dimensional compound ultrasound scans of the breast for refraction and motion correction. *Ultrasound Med Biol.* 1995; 21:769–78.
15. Rohling RN, Gee AH, Berman L. Automatic registration of 3-D ultrasound images. *Ultrasound Med Biol.* 1998;24:841–54.
16. Huber S, Wagner M, Medl M, et al. Real time spatial compound imaging in breast ultrasound. *Ultrasound Med Biol.* 2002;28: 155–63.
17. Weinstein SP, Conant EF, Sehgal C. Technical advances in breast ultrasound imaging. *Semin Ultrasound CT MR.* 2006;27:273–83.
18. Taki H, Sakamoto T, Yamakawa M, et al. Calculus detection for medical acoustic imaging using cross-correlation: simulation study. *J Med Ultrasonics.* 2010;37:129–35.
19. Taki H, Sakamoto T, Yamakawa M, et al. Small calculus detection for medical acoustic imaging using cross-correlation between echo signals. *Proc IEEE Int Ultrason Symp.* 2009; 2398–2401.